SLAC-PUB-14290

Electronic Structure of Crystalline ^{4}He at High Pressures

Ho Kwang Mao,[1,2,3] Eric L. Shirley,[4] Yang Ding,[2] Peter Eng,[5] Yong Q. Cai,[6] Paul Chow,[3] Yuming Xiao,[3] Jinfu Shu,[1] Russell J. Hemley,[1] Chichang Kao,[7,8] and Wendy L. Mao[9,10]

[1]*Geophysical Laboratory, Carnegie Institution of Washington, Washington, DC 20015, USA*

[2]*HPSynC and* [3]*HPCAT, Carnegie Institution of Washington, 9700 South Cass Avenue, Argonne, Illinois 60439, USA*

[4]*Optical Technology Division, National Institute of Standards and Technology, 100 Bureau Dr. MS 8441, Gaithersburg, Maryland 20899-8441, USA*

[5]*Consortium for Advanced Radiation Sources and James Franck Institute, University of Chicago, Chicago, Illinois 60637, USA*

[6]*National Synchrotron Light Source II, Brookhaven National Laboratory, Upton, New York 11973, USA*

[7]*National Synchrotron Light Source, Brookhaven National Laboratory, Upton, New York 11973, USA*

[8]*Stanford Synchrotron Radiation Laboratory, SLAC National Accelerator Laboratory, Menlo Park, CA 94025, USA*

[9]*Geological and Environmental Sciences, Stanford University, Stanford, CA 94305, USA*

[10]*Photon Science, SLAC National Accelerator Laboratory, Menlo Park, CA 94025, USA*

Using inelastic X-ray scattering techniques, we have succeeded in probing the high-pressure electronic structure of helium crystal at 300 K which has the widest known electronic energy bandgap of all materials, that was previously inaccessible to measurements due to the extreme energy and pressure range. We observed rich electron excitation spectrum, including a cut-off edge above 23 eV, a sharp exciton peak showing linear volume dependence, and a series of excitations and continuum at 26 to 45 eV. We determined electronic dispersion along the Γ-M direction over two Brillouin zones, and provided a quantitative picture of the helium exciton beyond the simplified Wannier-Frenkel description.

PACS numbers: 71.20.-b; 71.35.-y; 67.80.B-; 62.50.-p

Work supported in part by US Department of Energy contract DE-AC02-76SF00515.

SLAC National Accelerator Laboratory, Menlo Park, CA 94025

As an archetypal quantum solid that exhibits numerous singular, extreme properties, including the lowest freezing temperature [1], highest solidification pressure [2], extraordinary quantum effects [3, 4], and widest bandgap energy, condensed helium has been the focus of extensive recent studies (*e.g.*, Ref. [3-9]). Helium under high pressure-temperature conditions is also of great current interest to astrophysicists, as helium makes up a quarter of the mass of our solar system and the baryonic matter in the Universe [10]; the electron bandgap closure and metallization of helium may occur within many planets of Jupiter's mass and larger [11-14]. Our knowledge on high-pressure electronic structures of solid helium, however, is solely based on theoretical calculations; experimental determination has not been previously possible. Here we report the first direct measurement of electron excitations of single-crystal helium above 11 GPa, and present *ab-initio* calculations for comparison.

Helium has the highest ionization energy of all known materials, thus presenting an extraordinary experimental challenge. The energies of electron bandgap and associated excitations of solid helium are higher than 20 eV which is far beyond the optical range typically used for electronic measurements. Probing helium electron structure by one photon optical absorbance, reflectance [15], or fluorescence [16] spectroscopy requires vacuum ultraviolet photons at 20-40 eV that would be completely blocked by high-pressure window materials, as well as the bulk helium sample itself. Only the surface of condensed helium can be probed in near vacuum conditions [15], precluding high-pressure studies of bulk helium samples. This energy range can be accessed by the newly advanced, two-photon, inelastic, X-ray, scattering (IXS) spectroscopy [17] which uses high energy X-rays (~ 10^4 eV) to enter (with energy E) and exit (with energy E_0) the pressure vessel and sample. The electronic energy spectra in the 20-40 eV range are revealed by analyzing the X-ray energy loss between the two photons, *i.e.*, $\hbar\omega = E - E_0$. High-energy X-ray has an additional advantage in probing momentum transfer ($\boldsymbol{q}$) of electronic dynamics, while the optical ultraviolet photons can only probe the Brillouin zone center ($\boldsymbol{q} \approx 0$). The IXS double differential cross section is proportional to the dynamic structure factor

$$S(\mathbf{q},\omega) = \sum\nolimits_f \left|\langle f \left| e^{i\mathbf{q}\cdot\mathbf{r}} \right| I \rangle\right|^2 \delta(\hbar\omega - E_f + E_I) \qquad (1)$$

where *I* and *f* label the initial and final electronic states and their energies. As the second lightest element, however, helium has a very low X-ray scattering cross section, and its IXS signals are very weak even using high-brilliance synchrotron X-ray source. Previous IXS measurements of solid helium are therefore limited to relatively large samples (10 mm^3) in a beryllium cell at low pressures (<0.22 GPa) and temperatures (< 22 K) [5, 6, 17, 18].

At ambient temperature, diamond anvil cell (DAC) is the only apparatus to pressurize ^{4}He to reach the solidification pressure of 11 GPa and beyond [2]. The maximum sample size in DAC is small, *i.e.*, 10^{-4} times smaller than that in the low-pressure beryllium cell [17]. Although high-pressure electronic IXS spectroscopy in DAC has been developed for studying second-row elements [19-21], measurement of the weak signal from ^{4}He has proven challenging. We optimized the IXS-DAC technique at three third-generation synchrotron beamlines: 13ID-C [19] of the GeoSoilEnvironCARS (GSECARS) and 16ID-D [21] of the High Pressure Collaborative Access Team (HPCAT) at the Advanced Photon Source (APS), Argonne National Laboratory (ANL), and the Taiwan Beamline BL12XU [20] at SPring-8, Japan. To get sufficient counting statistics, we accumulated the signal and background for a total one-month of beam time.

We used a panoramic DAC [22] and maximized helium sample volume (10^{-3} mm^3) for the 10 - 20 GPa range using large diamond anvils of 630 μm culet diameter. A high-strength beryllium gasket (Grade I-250) with 5 mm outer diameter and 1 mm thickness [22] was fabricated to match the size and shape of diamond culets and to form a sample chamber of 180 μm inner diameter and 25 μm thickness. Research grade helium with natural isotopic abundance of ^{4}He (99.986%) was loaded in the DAC at 0.2 GPa at ambient temperature [23]. Pressure was calibrated by ruby fluorescence scale.

Both beamlines 13ID-C [19] and 16ID-D [21] at APS use Si(220) scanning incident X-ray monochromator, and an array of six spherical Si (660) analyzers (50 mm diameter) on a Rowland circle of 0.87-m diameter focusing to a single detector in back-scattering geometry (Bragg angle of 89°) at a fixed energy of E_0 = 9.6865 keV; the IXS spectrometer has 1 eV (FWHM) energy resolution [19]. Beamline BL12XU at SPring-8 uses Si (400) high-resolution scanning incident X-ray monochromator and two Si (555)

spherical analyzers on a Rowland circle of 2-m diameter at 9.8992 keV, achieving 175 meV energy resolution [20].

The ^{4}He sample was solidified at 11 GPa and grew into a hexagonal close-packed (hcp) single crystal [8, 23, 24], whose orientation was determined by X-ray diffraction [23, 24]. For direct comparison with optical spectroscopy, which samples the Brillouin-zone center, we measured IXS spectra near the Γ point of the first repetitive Brillouin zone. To minimize the background signals originating from IXS of beryllium and diamond, we focused the incident X-ray beam to restrict the beam cross-section within ^{4}He sample volume at all three beamlines. To block the detector from seeing the background signals along the X-ray beam path before and after the ^{4}He sample, we aligned a 150 μm-width receiving slit within 3 mm to the sample. The residual background signals from diamond anvils and Be gasket are significantly below the sample signals and can be fully subtracted based on the control IXS measurements of the adjacent diamond and Be regions. With the improved measurements, we are now able to observe many more features in the electronic structure of helium than previously possible [5, 6, 18]. Our IXS spectrum of ^{4}He at 13.4 GPa (Fig. 1) shows a wealth of information. In addition to the sharp exciton peak at 24.4 eV and the steep edge below 23.7 eV, for the first time we have observed a second broad, unresolved series of peaks around 27.5 eV, and a continuum at higher energy.

The sharp exciton peak was the only feature previously observed in helium at low pressure [5, 6, 18]. Two limiting cases have been used to describe excitons in noble-gas solids: Wannier exciton with freely mobile, weakly-bound electron and hole which is large, or Frenkel exciton with a more localized wave function that is smaller and tightly bound together. The ^{4}He exciton exhibits aspects of both types [18], Unable to see any $n \geq 2$ Wannier exciton, Arms *et al*. [5] suggested the exciton was a Frenkel exciton. Now with the clear presence of the series of unresolved peaks at 26-45 eV in our experiment, the possibility of Wannier series excitons mixing with interband transitions can no longer be dismissed. In any case, the Frenkel/Wannier distinction is somewhat artificial, and the onset of the continuum should have a smooth transition from the upper Rydberg-like excitons to unbound states. High pressures change length scales of both the excitonic

radii and the nearest neighbor atomic distance. It will be better to describe the system based on the full electronic spectrum, its dispersion, and its change under pressure.

We were able to obtain the full electronic IXS spectra over a range of pressure and momentum space. The ^{4}He exciton spectra along the Γ-M (h00) branch were measured by IXS at 11.9, 13.4, and 17.0 GPa, corresponding to molar volumes of 4.170, 4.000, and 3.696 cm^3/mol, and d_{100}-spacing (*i.e.*, spacing between two consecutive (100) atomic layers) of 1.853, 1.827, and 1.780 Å, respectively. The momentum transfer, (q) was calculated from the scattering angle (2θ) and X-ray wavelength (λ_0) or energy (E_0) by $q = (4\pi / \lambda_0)\sin\theta$, and the reduced momentum transfer along Γ-M in terms of the (100) reciprocal lattice vector is $q^* = q\ (d_{100}/2\pi)$. Fig. 2 shows the change of the $q^* = 1$, zone-center spectra as a function of pressure. The inset of Fig. 2 shows the pressure shift of the zone center exciton to lower energy with the molar volume (V) compression given by the linear relation:

$$E(\text{eV}) - E_0(\text{eV}) = 17.0(2) + 1.85(4)V(\text{cm}^3/\text{mol}) \qquad (5)$$

The 11.9 and 17.0 GPa spectra were obtained with 1 eV instrumental resolution at beamlines 13ID-C and 16ID-D, and the 13.4 GPa spectrum, with 175 meV resolution at beamline BL12XU [20]. The higher resolution of the latter showed a narrower exciton peak and improved resolution of features above 26 eV (Fig. 1), at the expense of a six-fold reduction in count rate. The 1 eV resolution is adequate for revealing many major features, including the cut-off edge, the sharp exciton, the series of unresolved excitations, and their shifts as a function of pressure and momentum transfer. We used the 1 eV resolution for better signal intensity and counting statistics to cover the wide range of pressure and momentum space, and the 175 meV resolution for verification of several key points.

We investigated the electron dynamics of hcp ^{4}He along the Γ-M (h00) direction at 11.9 GPa. Figure 3 (left) shows an extensive series of sixteen IXS measurements for 2θ ranging from 25° to 130° corresponding to the q^* range 0.628 to 2.628. The series was collected with the vertical-scattering spectrometer at 13ID-C, APS [19], as the horizontal-scattering spectrometers at 16ID-D, APS and BL12XU, SPring-8 with the horizontally polarized synchrotron X-ray sources were unsuitable for $2\theta > 60°$. The data quality was

at its best near the $q^* = 1$, Γ point at $30° < 2\theta < 50°$. At lower angles, the background from Be and diamond increased rapidly as the analyzer receiving slit approached the incident beam and lost its background discriminating capability. At higher angles, the IXS intensity diminished, and the collection time became exceedingly long.

With its closed 1*s* shell, ^{4}He is particularly amenable to theoretical calculations. We simulated the IXS spectra using *ab-initio* treatments of separate electron and hole dynamics and electron-hole interactions [25, 26] for the same pressure, Brillouin zone, and 2θ range as the experimental measurements. We calculated theoretical IXS spectra based on calculating the loss function. This relied on solution of the Bethe-Salpeter equation following the method of Benedict *et al*. [27], extended to finite momentum as by Caliebe *et al*. [28], and density-functional calculations in the local-density approximation using the plane-wave pseudopotential approach mimicking the methodology of earlier work [25]. We used a cut-off radius of 0.015 nm for the *s*-wave pseudopotential and a 400 Ry cutoff to ensure a realistic calculation. The band structure was corrected using Hedin's GW approximation for the electron self-energy [29] using the method of Hybertsen and Louie [30] for fcc He with a 64-point Monkhorst-Pack grid [31] and 45 bands included in the electron Green's function, cutoffs that have proven adequate for such wide-gap insulators with small unit cells. (In the GW approximation, the self-energy is the electron Green's function *G* times the screened Coulomb interaction *W*.) In fcc He at the same atomic volume, the correction was a 7% stretch of the occupied bands and 2% stretch of the unoccupied bands, with a widening of the band gap from about 17.1 eV to about 27.1 eV at all pressures considered here, and we safely extrapolated such effects to the similarly close-packed hcp structure. Over the same pressure range, the dielectric constant calculated in the GW calculations varied between 1.44 and 1.49, a reasonable value for the atomic density, and consistent with the values obtained from the Bethe-Salpeter calculations, in which we included 2 valence bands, 18 unoccupied bands, and up to 256 Brillouin-zone sampling points, which proved to be well converged.

Since pressure is a derivative of volume which is the more fundamental variable, the experimental results at 11.7 GPa are compared in Fig. 3 (left) with the theoretical calculations (left) at the same volume of 4.170 cm^3/mol. Both show a similar general spectral shape, relative intensity, and dispersion, indicating the robustness of the

calculations. The calculations resolve the multiple peaks revealed by the experiments, provide more details of the exciton beyond the simplified categorization of Frenkel and Wannier types. Agreement between theory and experiment also provides confidence for calculations at higher pressures and temperatures beyond the current experimental range. We identify the first peak that is strongest near $2\theta = 45°$ as an energetically isolated bound state. Core hole-excitonic effects are often very strong in wide gap insulators, so that other excitonic features appear merged with the continuum spectrum. As in other systems [32], a broad, structured feature appears to straddle the continuum threshold.

The experimental and theoretical dispersions of the first excitonic peak as a function of the momentum transfer in the Γ-M branch are plotted in Fig. 4. Our experiment clearly identifies the energy minimum at the zone center (Γ-point) and a maximum at the zone edge (M-point) of the repetitive periodic Brillouin zones. The large dispersion amplitude (about 1.5-2 eV) for $q^* = 0.628$ to 1.0 is in good agreement with the calculation. The information from first Brillouin zone is accurate and sufficient to show the amplitude of the periodic dispersion. The 0.5 eV offset between theory and experiment reflects the uncertainty which is dwarfed by the correlation and excitonic binding effects on the excitation energy (about 4.5 eV and 3.5 eV, respectively). For $q^* > 1.3$ due to the diminishing exciton peak intensity and overlapping with the rising edge of features at higher energy (Fig. 3), the exciton peak is increasingly difficult to resolve and its position is uncertain. Nevertheless, the maximum and minimum are still visible qualitatively.

This research was carried out as part of the EFree, an Energy Frontier Research Center funded by the U.S. Department of Energy (DOE), Office of Science, Office of Basic Energy Sciences (BES) under Award Number DE-SC0001057 and the Division of Material Science and Engineering under Contract No. DE-AC02-76SF00515. The use of HPCAT (Sector 16) is supported by CIW, CDAC, UNLV and LLNL through funding from DOE-NNSA, DOE-BES and NSF; the use of GSECARS is supported by the NSF EAR-0622171 and DOE - Geosciences DE-FG02-94ER14466; the use of BL12XU, SPring-8, is supported by the National Synchrotron Radiation Research Center and National Science Center of Taiwan. APS is supported by DOE-BES, under Contract No. DE-AC02-06CH11357.

References

[1] M. A. Adams, J. Mayers, O. Kirichek, and R. B. E. Down, Phys. Rev. Lett. **98**, 085301 (2007).

[2] J. M. Besson, and J. P. Pinceaux, Science **206**, 1073 (1979).

[3] E. Kim, and M. H. W. Chan, Science **305**, 1941 (2004).

[4] E. Kim, and M. H. W. Chan, Nature **427**, 225 (2004).

[5] D. A. Arms, R. O. Simmons, M. Schwoerer-Böhning, A. T. Macrander, and T. J. Graber, Phys. Rev. Lett. **87**, 156402 (2001).

[6] D. A. Arms, T. J. Graber, A. T. Macrander, R. O. Simmons, M. Schwoerer-Böhning, and Y. Zhong, Phys. Rev. B **71**, 233107 (2005).

[7] C.-S. Zha, H. K. Mao, and R. J. Hemley, Phys. Rev. B **70**, 174107 (2004).

[8] Z. Nabi, L. Vitos, B. Johansson, and R. Ahuja, Phys. Rev. B **72**, 172102 (2005).

[9] Y. A. Freiman, S. M. Tretyak, A. Grechnev, A. F. Goncharov, J. S. Tse, D. Errandonea, H. K. Mao, and R. J. Hemley, Phys. Rev. B **80**, 094112 (2009).

[10] W. B. Hubbard, A. Burrows, and J. I. Lunine, Annu. Rev. Astron. Astrophys **40**, 103 (2002).

[11] A. Kietzmann, B. Holst, R. Redmer, M. P. Desjarlais, and T. R. Mattsson, Phys. Rev. Lett. **98**, 190602 (2007).

[12] S. A. Khairallah, and B. Militzer, Phys. Rev. Lett. **101**, 106407 (2008).

[13] D. J. Stevenson, Proc. Nat. Acad. Sci. USA **105**, 11035 (2008).

[14] L. Stixrude, and R. Jeanloz, Proc. Nat. Acad. Sci. USA **105**, 11071 (2008).

[15] C. M. Surko, G. J. Dick, and F. Reif, Phys. Rev. Lett. **23**, 842 (1969).

[16] M. Joppien, R. Karnbach, and T. Möller, Phys. Rev. Lett. **71**, 2654 (1993).

[17] W. Schülke, A. Kaprolat, K. J. Gabriel, N. Schell, E. Burkel, and R. O. Simmons, Rev. Sci. Instrum. **66**, 1578 (1995).

[18] N. Schell, R. O. Simmons, A. Kaprolat, W. Schülke, and E. Burkel, Phys. Rev. Lett. **74**, 2535 (1995).

[19] W. L. Mao, H. K. Mao, P. Eng, T. Trainor, M. Newville, C. C. Kao, D. L. Heinz, J. Shu, Y. Meng, and R. J. Hemley, Science **302**, 425 (2003).

[20] Y. Q. Cai, H. K. Mao, P. C. Chow, J. S. Tse, Y. Ma, S. Patchkovskii, J. F. Shu, V. Struzhkin, R. J. Hemley, H. Ishii, C. C. Chen, I. Jarrige, C. T. Chen, S. R. Shieh, E. P. Huang, and C. C. Kao, Phys. Rev. Lett. **94**, 025502 (2005).

[21] W. L. Mao, H. K. Mao, Y. Meng, P. Eng, M. Y. Hu, P. Chow, Y. Q. Cai, J. Shu, and R. J. Hemley, Science **314**, 636 (2006).

[22] H. K. Mao, J. Xu, V. V. Struzhkin, J. Shu, R. J. Hemley, W. Sturhahn, M. Hu, E. Alp, L. Vocadlo, D. Alfè, G. D. Price, M. J. Gillan, M. Schwoerer-Böhning, D. Häusermann, P. Eng, G. Shen, H. Giefers, R. Lübbers, and G. Wortmann, Science **292**, 914 (2001).

[23] H. K. Mao, R. J. Hemley, Y. Wu, A. P. Jephcoat, L. W. Finger, C. S. Zha, and W. A. Bassett, Phys. Rev. Lett. **60**, 2649 (1988).

[24] P. Loubeyre, R. LeToullec, J. P. Pinceaux, H. K. Mao, J. Hu, and R. J. Hemley, Phys. Rev. Lett. **71**, 2272 (1993).

[25] E. L. Shirley, Phys. Rev. B **58**, 9579 (1998).

[26] E. L. Shirley, Phys. Rev. Lett. **80**, 794 (1998).

[27] L. X. Benedict, and E. L. Shirley, Phys. Rev. B **59**, 5441 (1999).

[28] W. A. Caliebe, J. A. Soininen, E. L. Shirley, C.-C. Kao, and K. Hämäläinen, Phys. Rev. Lett. **84**, 3907 (2000).

[29] G. Onida, L. Reining, and A. Rubio, Rev. Mod. Phys. **74**, 601 (2002).

[30] M. S. Hybertsen, and S. G. Louie, Phys. Rev. B **34**, 5390 (1986).

[31] H. J. Monkhorst, and J. D. Pack, Phys. Rev. B **13**, 5188 (1976).

[32] J. A. Soininen, and E. L. Shirley, Phys. Rev. B **64**, 165112 (2001).

Figure Captions

Figure 1. ^{4}He zone -center IXS spectra and background at 13.4 GPa. The raw spectrum contains background contribution from Be and diamond. Moving the X-ray beam 100 μm into the pure Be gasket area, we collected a typical metallic spectrum with initial slope taking off from zero energy loss. Moving the X-ray beam 100 μm into the upper or lower diamonds, we collected insulator spectra with initial slope taking off above 10 eV. The backgrounds are subtracted by matching slopes of the raw spectrum at zero and 10 eV with a fraction of the Be and diamond spectra to obtain the net ^{4}He IXS spectrum.

Figure 2. ^{4}He zone-center IXS spectra at high pressures. IXS measurement cannot be obtained at the exact Γ-point where the intense elastic scattering from the 100 Bragg diffraction swamps the weak IXS spectra. Our measurements were taken slightly off the Γ-point at $2\theta = 40°$, corresponding to $q^* = 0.992$, 0.998, and 0.972 for measurements at 11.9, 13.4 , and 17 GPa, respectively. Inset, exciton peak position as a function of molar volume.

Figure 3. Experimental (left) and theoretical (right) IXS spectra of ^{4}He at the volume of 4.170 cm^3/mol. Dispersion along the *h*00 direction, IXS spectra are shown with scattering angle from 25° to 90° in 5° steps and 90° to 130° in steps of 20°. Dotted gray lines are a guide for the eye.

Figure 4. Dispersion of the ^{4}He exciton along periodic Brillouin zone Γ (q* = 1 and 2) to M (q* = 0.5 and 1.5) at the volume of 4.170 cm^3/mol.

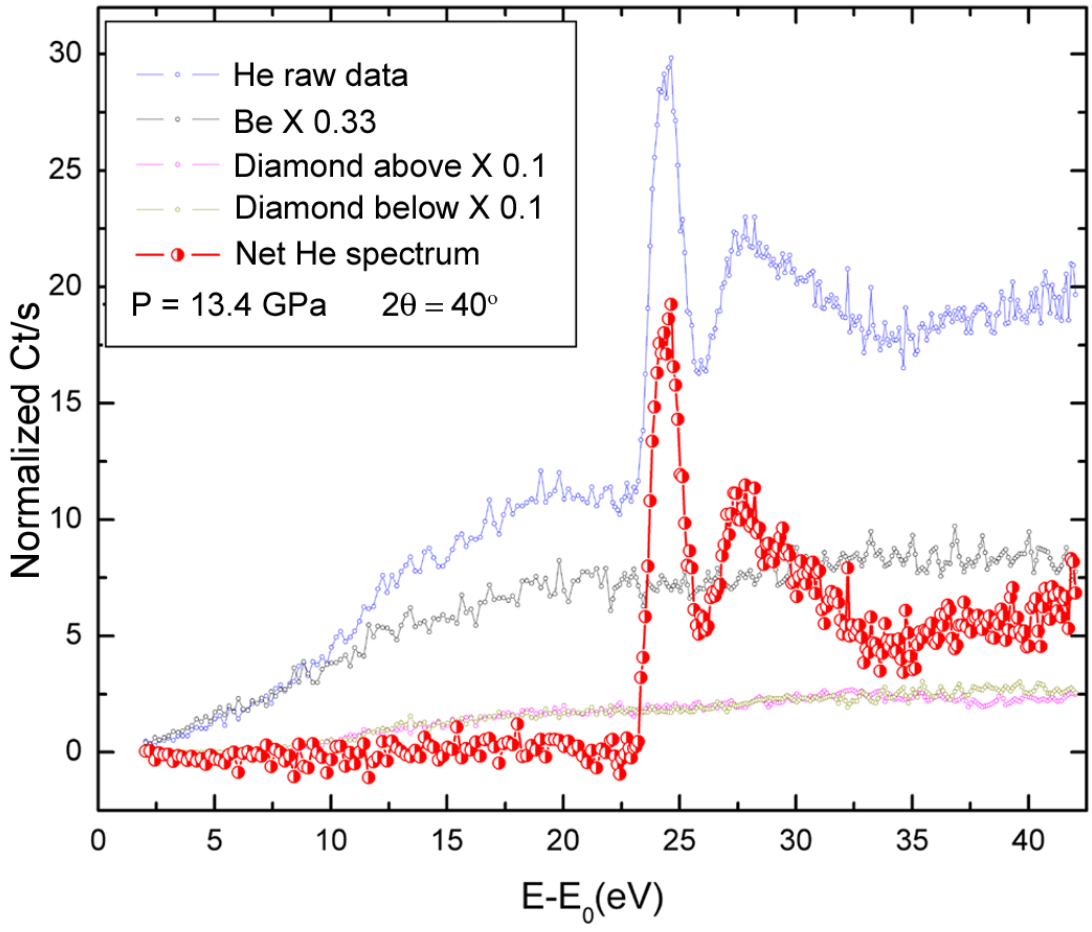
He raw data
Be X 0.33
Diamond above X 0.1
Diamond below X 0.1
Net He spectrum
P = 13.4 GPa
2θ = 40°
Normalized Ct/s
E-E0(eV)
0
5
10
15
20
25
30
35
40

Figure 1.

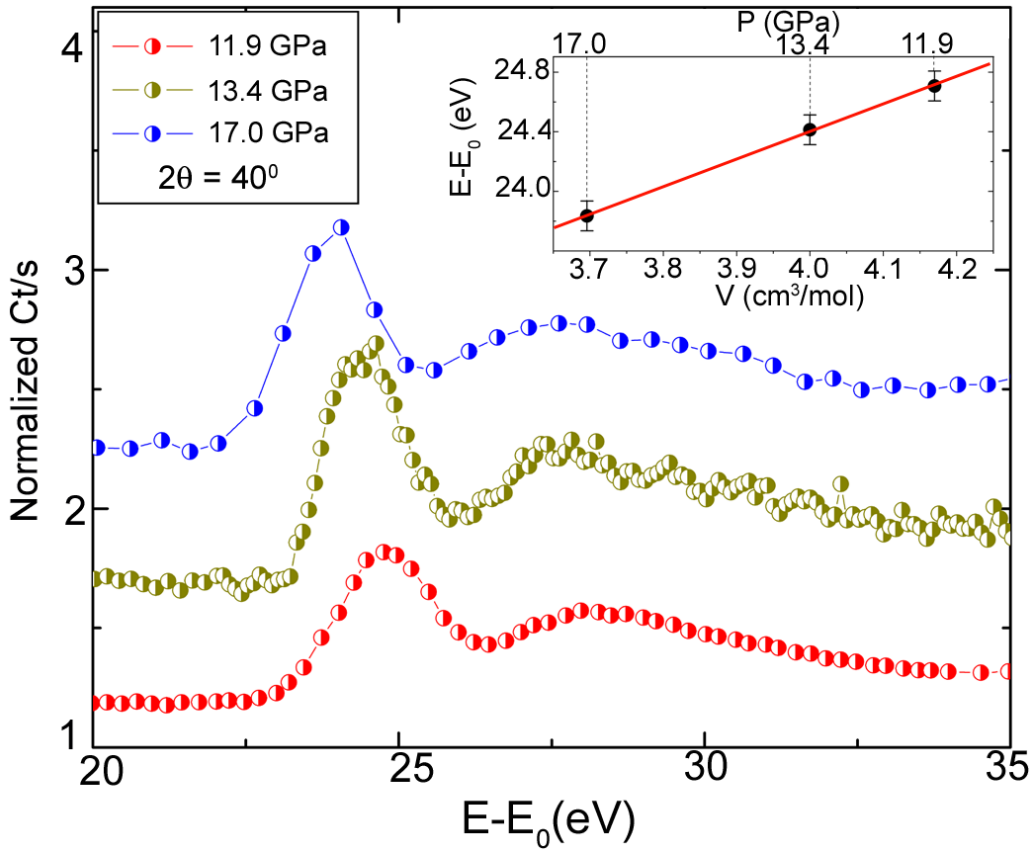
11.9 GPa
13.4 GPa
17.0 GPa
2θ = 40⁰
P (GPa)
17.0
13.4
11.9
E-E0 (eV)
24.8
24.4
24.0
3.7
3.8
3.9
4.0
4.1
4.2
V (cm³/mol)
Normalized Ct/s
4
3
2
1
20
25
30
35
E-E0(eV)

Figure 2.

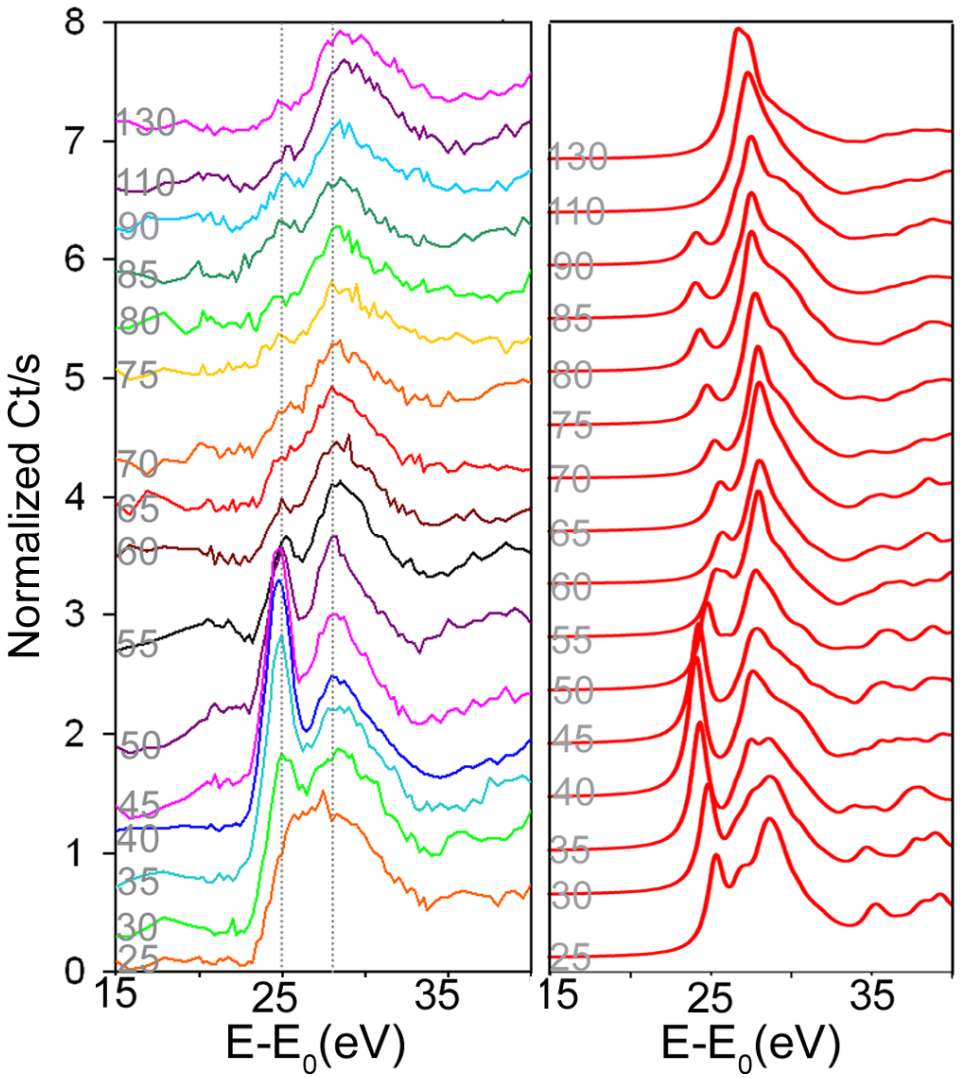
Normalized Ct/s
E-E0(eV)
E-E0(eV)
130
110
90
85
80
75
70
65
60
55
50
45
40
35
30
25

Figure 3.

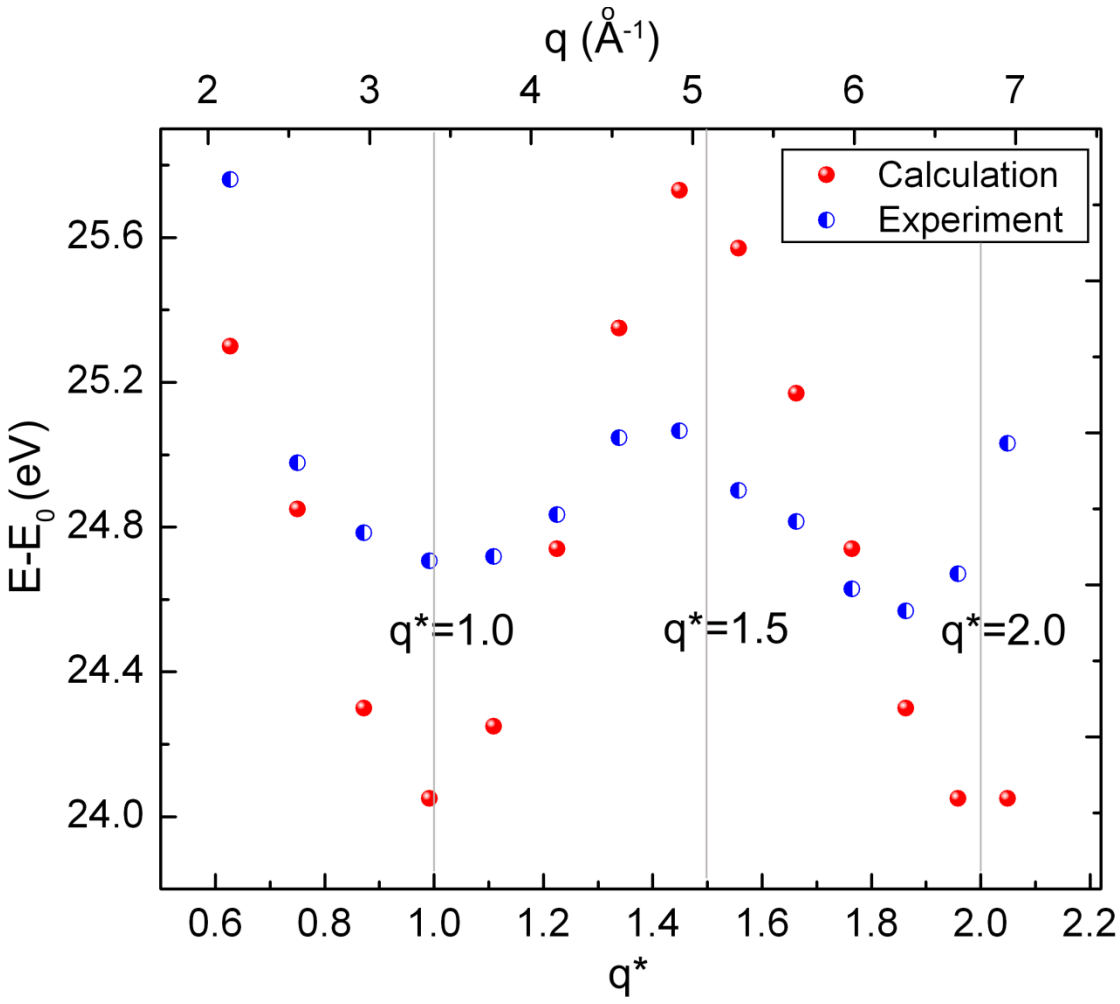
q (Å-1)
2
3
4
5
6
7
Calculation
Experiment
25.6
25.2
24.8
24.4
24.0
E-E0 (eV)
q*=1.0
q*=1.5
q*=2.0
0.6
0.8
1.0
1.2
1.4
1.6
1.8
2.0
2.2
q*

Figure 4.